THE ASTROPHYSICAL JOURNAL, 436:859–870, 1994 December 1


# LINE PROFILE VARIATIONS FROM ATMOSPHERIC ECLIPSES: CONSTRAINTS ON THE WIND STRUCTURE IN WOLF-RAYET STARS

L. H. AUER
ESS-5, MS F665, Los Alamos National Laboratory, Los Alamos, NM 87545
AND
G. KOENIGSBERGER
Instituto de Astronomía, UNAM, Apdo. Postal 70-264, Mexico D.F. 04510, Mexico
*Received 1993 December 17; accepted 1994 June 1*

## ABSTRACT

Binary systems in which one of the components has a stellar wind may present a phenomenon known as "wind" or "atmospheric eclipse," in which that wind occults the luminous disk of the companion. The enhanced absorption profile, relative to the spectrum at uneclipsed orbital phases, can be modeled to yield constraints on the spatial structure of the eclipsing wind. A new, very efficient approach to the radiative transfer problem, which makes no requirements with respect to monotonicity of the velocity gradient or the size of that gradient, is presented. The technique recovers both the comoving frame calculation and the Sobolev approximation in the appropriate limits. Sample computer simulations of the line profile variations induced by wind eclipses are presented. It is shown that the location of the wind absorption features in frequency is a diagnostic tool for identifying the size of the wind acceleration region. Comparison of the model profile variations with the observed variations in the W-R + 6 binary system V444 Cyg illustrate how the method can be used to derive information on the structure of the wind of the W-R star and constrain the size of the W-R core radius.

*Subject headings:* binaries: eclipsing — line: profiles — stars: individual (V444 Cygni) — stars: mass loss — stars: Wolf-Rayet

## 1. INTRODUCTION

Wolf-Rayet (W-R) stars form a class of evolved, early-type stars with extremely high mass-loss rates, in a range of 2–4 $\times 10^{-5}\ M_{\odot}$ year$^{-1}$ (Barlow, Smith, & Willis 1981). The origin of these mass-loss rates is still uncertain, although radiative forces seem to be a sufficient momentum-deposition mechanism (Lucy & Abbott 1993). However, a more precise determination of the driving mechanisms is hampered by the lack of a more detailed knowledge of the dynamics and structure of these winds.

Recent developments in the treatment of radiative transfer in W-R stars provide one set of diagnostics for the intrinsic wind properties (Hamann 1985; Hamann & Schmutz 1987; Schmutz, Hamann, & Wessolowski 1989; Hillier 1983; 1987a, b; 1989; and review by Kudritzki & Hummer 1990). There are, however, potential difficulties with the use of such tools. First, the data represent a three-dimensional integral over the emitting volume. This averages the location of the sources of spectral features over the corresponding velocity surfaces and limits the resolution of the diagnostics. Second, the true distance scale within the wind is an indeterminate quantity in these analyses, which likewise introduces uncertainty in the results; that is, the location of the gas causing the spectra is not fixed by the modeling relative to the center of the star, but with respect to the W-R continuum-emitting core radius, the dimensions of which are not well defined. As noted by Hillier (1991) in a recent review of the standard model, models with different combinations of core radii and velocity laws lead to observationally indistinguishable continuum distributions and line profiles. Furthermore, this ambiguity in the core radius makes it impossible to relate the W-R stars to the evolutionary models of post–main-sequence massive stars in a reliable manner. Clearly, the solution to this problem is to devise a method to constrain the velocity law and to establish an absolute distance within the W-R wind.

Binary systems in which the orbital parameters are well determined provide the required "yardstick" for establishing an absolute distance scale within the wind, and the line profile variations which occur as a result of the wind eclipse of the comparison O-star can be used to constrain the structure of the W-R wind. This approach of using a binary companion to obtain information on the atmosphere of a star has been used successfully in the case of late-type stars (see Reimers 1987, and references therein).

The presence of atmospheric eclipses in the continuous spectrum of V444 Cyg was first recognized by Kopal & Shapley (1946), who concluded that the effect was due to an extended electron scattering envelope around the W-R component of the system. Münch (1950) found, in addition, enhanced absorption associated with the emission lines when the O-star is on the far side of the wind, concluding that this was a result of atmospheric eclipses at line frequencies. Atmospheric eclipses were first detected in the far UV spectral region in *IUE* spectra of $\gamma^2$ Vel (Willis et al. 1979), where they were used to derive an estimate of the density of C III ions in the WC star's wind. Most of the galactic W-R systems thus far observed with *IUE* present the effect, to some degree or other (see Koenigsberger 1990 and references therein) as do two systems in the SMC (Moffat, Koenigsberger, & Auer 1989).

It is important to note that in close binaries where both components possess stellar winds, a wind-wind collision is predicted to occur (Pilutskii & Usov 1976), and several calcu-

lations of this effect have been performed (Stevens 1993 and references therein; Shore & Brown 1988; Lou, McCray, & Mac Low 1990).

However, the wind-wind collision appears to be a second-order effect, compared to the wind eclipse, in terms of producing the observed line-profile variability in the UV. This assertion is based on the low-dispersion *IUE* observation of six WN systems by Koenigsberger & Auer (1985) where the phase-dependent variations in the N IV 1718 Å line are found to be very similar in the five well-known binaries, despite different orbital separations, and different O-type companions. Specifically, the ratio of absorption ($W_A$) to emission ($W_E$) component equivalent width of N IV 1718 Å increases significantly at phases $0.85 \leq \phi \leq 0.15$ (O-star in back of W-R wind), with respect to all other phases for the five systems, with very similar amplitudes in all cases. The sixth system, HD 193077 (= WR 138) is believed to be a very long period system (Annuk 1991) and no significant variations in $W_A/W_E$ were detected. The value of $W_A/W_E$ for HD 193077 is the same as that of the other five systems at orbital phases outside of wind eclipse and secondary eclipse. Furthermore on the high-resolution spectra the normalized profile of N IV 1718 Å in V444 Cyg at phase $\phi = 0.74$ and HD 193077 are quite similar, except for the flux values at emission and absorption component line centers. V444 Cyg has slightly weaker emission and stronger absorption than HD 193077. Hence, adopting the N IV 1718 Å profile of HD 193077 as the intrinsic W-R P Cygni profile, one is led to conclude that the profiles of the other systems are affected by enhanced absorption when the O-star is occulted by the W-R wind, i.e., wind eclipse.

If one assumes that the phase-dependent variations result exclusively from the wind eclipse mechanism, then it is possible to associate the observed profile variations with changes in the wind structure along each ray as a function of orbital phase. This allows a constraint to be placed on the physical position within the wind of the absorbing/emitting gas and on the manner in which the velocity and density structures change with distance from the W-R core. Thus, the change in the P Cygni structure of the line, from one orbital phase to another, provides information on the change in the structure of the wind from one orbital impact parameter to another.

In order to be able to interpret the observations, it is necessary to model the effects due to atmospheric eclipse. In this paper we present the method and the results of computations of phase-dependent profile variations and show that these can be used to constrain the velocity law within the wind.

## 2. MATHEMATICAL MODELING OF THE WIND ECLIPSE

In our modeling of the eclipse of the companion by the W-R wind, we have been guided by the desire to establish constraints on the structure of the wind. That is, we are more interested in the general features of the wind than in detailed fits. We have accordingly made relatively simple assumptions about the structure of the absorbing region. Because of the high velocity in the wind, the dominant terms determining the spectra are the Doppler shift of the line profiles and the variation of the opacity in the wind. As long as these are adequately included, we may be relatively crude in our treatment of the other aspects of the radiative transfer problem and still obtain the desired constraints on the wind structure. To the extent that our simple models predict the eclipses, they place important constraints on the structure. To the extent that they do not fit, they give insight into the details of the winds in these relatively close binary systems.

There are three basic terms which determine the observed flux as a function of the eclipse phase: (1) the emission by the W-R and its associated wind; (2) the flux from the O-star, part of which may be absorbed by the material between the observer and the companion; and (3) the radiation from the wind that is occulted by the O-star. We will ignore the possible lines arising in the wind of the O-star. As a function of time the total flux is, thus,

$$F_{\rm tot}(x, t) = F_{\rm wr+wind}(x) + \langle F_{\rm O}(x) \exp\{-\tau[x, p(t)]\} - \langle F_{\rm wr-occ}(x, t)\rangle \rangle , \quad (1)$$

where the angle brackets indicate integration over the O-star disk; $x$ is the nondimensional frequency $\Delta v/\Delta v_D$; and $p(t)$, which is the orbital impact parameter at orbital phase $t$, is the minimum distance from the primary to the line of sight to the secondary. The usual $(p, z)$ coordinate system is used (Mihalas 1978) and is illustrated in Figure 1.

The first term in equation (1) is the integral over the W-R and its wind, while the second term is the integral over the surface of the O-star as attenuated by that wind. The third term is just the wind emission occulted by the companion at

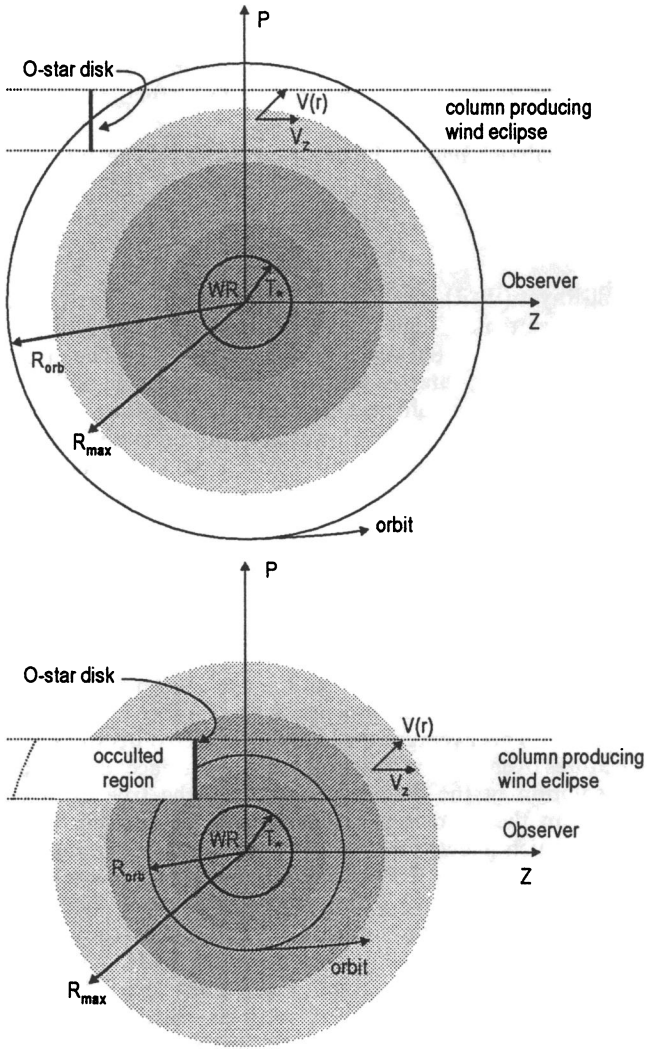


FIG. 1.—Schematic illustration of the geometry assumed for the model calculations. In Fig. 1*a*, the O-star orbit lies beyond the region of line formation, while in Fig. 1*b* it is immersed in it.

time $t$. In our analysis we assume that the first term does not depend on the phase in the orbit. There are, of course, potential interactions of the O-star with the wind that would introduce such a phase dependence. For example, the O-star could affect the dynamics of the wind either by direct radiative acceleration, or by interaction of the O-star's wind with the W-R wind, or by establishing a turbulent wake as it moves through the wind. On the other hand, there could be a purely radiative effect because the amount of O-star radiation which is scattered—as opposed to absorbed—by the wind depends on the phase. As we discussed above, in the present analysis we are ignoring these effects in the modeling in order to obtain a relatively simple parameterization of the phenomenon.

The second term in equation (1) is highly dependent on the orbital phase. The absorption depends on the column integral through the wind up to the O-star, which clearly varies during the orbit. This positional dependence appears as the indicated variation of $\tau$ as a function of the impact parameter, $p(t)$. From the variation of the profile with phase we can empirically determine $\tau[x, p(t)]$. Because the orbital elements of the system are known, we can determine the actual physical path through the wind that is causing $\tau[x, p(t)]$, and by combining the two we obtain our constraints on the structure of the wind.

The third term is likewise phase dependent but is complementary to the variation of the second term. Because it is caused by the occultation of the material on the far side of the companion, its effect appears at the velocities corresponding to the "far side" of the wind, while the "wind eclipse" occurs at velocities occurring in the "near side" of the wind. A priori, one also expects the size of the third term to be smaller than that due to the wind eclipse of the companion. The argument for this is the fact that there is an absorption component in the P Cygni profiles. This can occur only if the wind is not as bright as the star, i.e., that absorption dominates the partially compensating wind emission. Indeed, the models show that this term's contribution is almost two orders of magnitude smaller.

Correct computation of the first and third terms in equation (1) requires the solution of the multilevel non-LTE transfer problem in the moving medium. This, of course, is a well-studied problem, but there are still uncertainties in the solution, from both the atomic and physical modeling, that we would like to avoid. In our current modeling effort we have assumed that the source function is constant through the wind. We can minimize the importance of this approximation by using the flux relative to some standard phase for the modeling. By this means, the majority of the wind emission is cancelled leaving only the effects of the second and third terms.

To the extent that the W-R flux is not intrinsically phase dependent, the flux difference varies as

$$\begin{aligned}\Delta F(x, t) &= F(x, t) - F(x, t_0) \\ &= \langle F_O(x) \exp\{-\tau[x, p(t)]\}\rangle \\ &\quad - \langle F_O(x) \exp\{-\tau[x, p(t_0)]\}\rangle \\ &\quad - \langle F_{wr-occ}(x, t)\rangle + \langle F_{wr-occ}(x, t_0)\rangle . \end{aligned} \quad (2)$$

To first order, the time dependence of the change in the profile is a function only of the column integral up to and beyond the O-star. This means that by fitting $\Delta F$ we obtain directly information on the variation of the velocity and opacity along the column crossing the wind and passing through the companion. We emphasize that the importance of using $\Delta F$ instead of $F$ is due to the fact that this eliminates the intrinsic profile and thus isolates and accentuates the contributions from the column of material toward the O-star. The uncertain intrinsic profile is therefore cancelled out. The phase-dependent variation of $\Delta F$ can be calculated by a simple integral in the direction of the O-star once the impact parameter, $p(t)$, is known from the orbital phase, and the variation of velocity, $v_z(z)$, and opacity, $\chi(z)$, are specified along the line of sight.

In order to parameterize the computation of $\Delta F$, we make the following assumptions: the wind is spherically symmetric, its structure does not depend on the orbital phase, and we ignore the details of the variations of the O-star flux profile across its surface, i.e., limb darkening. The variation of the opacity involves both the change in the total density as well as the state of the gas. Accordingly, we have parameterized the opacity by $\chi(r) = X(r)/[v(r)r^2]$, with $X(r)$ an arbitrary function whose value is determined by fitting the data.

A new, very efficient method has been developed for solving the formal radiative transfer problem in the presence of velocity fields. (Although the formal solution is all that is required to determine $\Delta F(x, t)$ in eq. [2], we should note the same approach has also been successfully used in the solution of the multilevel non-LTE case; Auer & Dickel 1994.) The key to the efficiency of the method is the observation that although the full line width may be hundreds of times the Doppler line width, as we integrate across a cell we only have to solve the formal transfer equation at frequencies where there is opacity in that layer. This typically will be a very small fraction of the total line width (as viewed by an outside observer). This simple trick automatically achieves the economy of solution in the comoving frame, but maintains the simplicity of lab-frame solution at the cost only of sufficient storage for the profile at one spatial point. (For the non-LTE scattering problem, not being addressed here, one needs to store only the integrals over frequency as functions of position. The emergent intensity profile, which of course is the desired quantity, is simply the final value in the profile array used in the sweep along the ray). A very important aspect of the method is that it makes no requirements with respect to monotonicity of the velocity gradient or the size of that gradient. The technique is, thus, significantly more general and robust than either the comoving frame calculation or the Sobolev approximation, recovering both in the appropriate limits.

In greater detail, in making the calculation we divide the wind into radial shells, $r(k)$, $(k = 1, \ldots, N)$, with corresponding values for the nondimensional velocity, $(v_r)k$, which is measured in units of the thermal velocity, and opacity, $\chi(k)$. This defines the parameterized structure of the wind. For the phase with impact parameter $p$, we compute the values at the intersection of the ray and the radial grid of

$$\begin{aligned} z(k) &= \sqrt{[r(k)^2 - p^2]}\,, \\ v_z(k) &= \frac{v_r(r)z(k)}{r(k)}\,, \\ \chi(k) &= \chi[r(k)] \end{aligned} \quad (3)$$

up to the position of the O-star, with $z(k) < 0$ if the intersection is beyond the tangent point (i.e., the "far" side of the wind, with respect to the observer). The problem is to integrate over $z$ to find the optical depth to the O-star. We have assumed (1) Doppler line profiles, (2) piecewise linear variation of $v_z(z)$, and (3) that $\chi(r)$ varies across the cell as a piecewise continuous power law in $r$ [that is, $\chi(r) = \chi_0(k)r^{\beta(k)}$, where $\chi_0(k)$ and $\beta(k)$ are

chosen to recover the grid values]. Analytically we have

$$\tau(x) = \int \chi[r(z)]\phi[x - v_z(z)]dz \,, \tag{4}$$

where here $\phi$ is the profile function, $x$ is the frequency, and $v_z$ is the velocity measured in Doppler units. This integral can be evaluated numerically across the $k$th layer. We use two approaches depending on the size of the velocity shift across the layer, $\Delta v_z = |v_z(k+1) - v_z(k)|$. If $\Delta v_z < 1$ we may simply use Gaussian quadrature directly to evaluate the integral because the dominant change in the integrand is due to the smooth power-law variation of the opacity. For higher velocity gradients, we make a change of variables. Defining $q(z) = x - v_z(z)$, we obtain the new variable of integration for the layer,

$$e(z) = \int_{q[z(k)]}^{q[z(k+1)]} \phi(q')dq' \,. \tag{5}$$

Because the variation of $v_z(z)$ across the cell is approximated as a linear function of $z$, we obtain

$$\tau(x) = \frac{1}{(dv_z/dz)} \int \chi[r(e)]de \,, \tag{6}$$

where $r(e)$ is obtained from the fact that $q$ is a linear function of $z$, and $q(e)$ is simply the inverse function of equation (5), which may be approximated by an accurate polynomial fit. In order to evaluate equation (6), we again use Gaussian quadrature, but now applied to the interval $e(k)$, $e(k+1)$. This approach recovers the properly centered Sobolev limit for large velocity gradients and is, of course, exact within the approximation that the velocity gradient is linear across the cell. Any inaccuracy caused by this point is mitigated simply by using more radial grid points. Formal solution for $F(x)$ is now trivial. We initialize $F(x) = F_{O*}$ and then step over each shell in the radial grid intersected by the ray with impact parameter $p$. For the $k$th layer, we need to evaluate equation (6) only at frequencies in the range $v_{min} = \{\min [v_z(k), v_z(k+1)] - \text{line width}\}$ to $v_{max} = \{\max [v_z(k), v_z(k+1)] + \text{line width}\}$, where for Doppler line profiles we have used a line width of $\sim 3.5$ as the limit beyond which there is negligible contribution to the optical depth. (If Voigt profiles were used a much larger line width would be required.) If the array, $F(i)$, is used to store the profile at equal steps in the Doppler width, the range of subscripts is simply found by dividing $v_{min}$ and $v_{max}$ by that spacing. At these frequencies we update

$$F(x, p) \rightarrow F(x, p) \exp [-d\tau(x)] \,. \tag{7}$$

When we reach the outmost shell, the array $F(x, p)$ will contain all the profile information we need to evaluate $\Delta F(x, p)$. Thus, we can compute the profile differences.

The method is entirely general and any velocity law can be used.

## 3. MODEL COMPUTATIONS

The primary objective of the modeling efforts we present in this section is to obtain a set of diagnostics which may be used to constrain the velocity law of the W-R wind. Specifically, as a first approximation to the velocity law, it is desirable to determine the physical extent of the wind region which is undergoing an acceleration. Thus, any diagnostic which differentiates an accelerating wind from one which is expanding at constant velocity will provide the desired constraints. In addition, the limitations of the diagnostics as well as the dependence on other parameters of the system must be understood.

Given that our primary objective at this stage is to differentiate between an accelerating and a constant velocity flow, we have used the simplest possible parameterization for the velocity law: piecewise linear, with acceleration out to some specified radius $R_a$, and then a constant velocity. Although simplistic, this law allows us to address the question of the size of the region of acceleration.

In Table 1 we define the input parameters which determine each model. The number of radial (nr) and frequency (nx) grid points used was 95 for all computations. The remaining parameters can be divided into two groups: (1) the parameters which determine the W-R wind structure and the emergent line profile [$R_{max}$, $V_{max}$, $R_a$, $X(r)$, and $F_{wr}$]; and (2) the parameters related to the binary nature of the system ($R_{orb}$, and $V_{orb}$) and the O-star companion's characteristics ($R_{O*}$, $F_{O*}$). In principle, the parameters of the second group can be derived from radial velocity variations and light curves and are assumed to be known. From the first group, we can ignore $F_{wr}$ since the dependence on this parameter is eliminated when the difference of two profiles is computed (cf. equation [2]). Furthermore, $V_{max}$ is the maximum speed achieved within the wind, a quantity which can be derived from the observed line profiles. Thus, the free parameters for the simulations are $R_{max}$, the maximum extent of the line emitting region; $R_a$, the distance over which an acceleration is occurring; and $X(r)$, the scaled monochromatic opacity of the emission line being modeled. All parameters are nondimensional: distances are in units of $r_*$, which is the position where the acceleration is presumed to start, and speeds are in units of the Doppler speed. Figure 1 illustrates schematically the relative distances, and two scenarios: the O-star orbit larger (*top*) and smaller (*bottom*) than the size of the line-forming region.

Once the input parameters have been specified, a model run consists of the computation of the W-R (intrinsic) line profile, followed by the computation of the emergent line profile produced by the transfer of the radiation of the O-star through different columns of W-R wind; each column corresponds to an orbital phase of the system. Finally, the differences of the profiles at phases $t_1$, $t_2$, ..., and the profile at the reference phase $t_0$ are plotted. The phase convention we use here is as follows: $t_0 = 0.75$ and corresponds to the elongation at which the O-star is receding from the observer, and at which the orbital impact parameter is largest; $t_1$, $t_2$, ... are phases $0.75 < t < 1.00$, at which an atmospheric eclipse occurs. For each model we have computed the difference $\Delta F(x, t) = F(x, t) - F(x, t_0)$ with $t = 0.85, 0.89, 0.92, 0.96, 0.98$ as representative phases. These phases correspond to orbital impact parameters $p/r_* = 8.1$, 6.4, 4.8, 2.5, and 1.2, for an orbital separation $R_{orb}/r_* = 10$; and $p/r_* = 24.3$, 19.1, 14.5, 7.5, and 3.8 for an orbital separation $R_{orb}/r_* = 30$.

TABLE 1

DESCRIPTION OF INPUT PARAMETERS OF THE CODE

| Parameter | Description |
|---|---|
| $R_{max}$ ..... | Maximum extent of line-emitting region, in stellar radii units |
| nr, nx ..... | Number of radial and frequency grid points |
| $V_{max}$ ..... | Maximum expansion velocity, in Doppler velocity units |
| $R_a$ ..... | Acceleration radius, in stellar radii units |
| $X(r)$ ..... | Monochromatic opacity function |
| $F_{wr}$ ..... | Continuum flux of W-R star emerging from $r = 1r_*$ |
| $F_{O*}$ ..... | Flux of O-Star's radiation |
| $R_{orb}$ ..... | Orbital separation |
| $R_{O*}$ ..... | Radius of O-star companion |
| Vel ..... | Orbital velocity, in thermal velocity units |
| $t_0$ ..... | Reference phase |
| $t_i$ ..... | Set of $i$ phases to produce profile differences |

TABLE 2

INPUT PARAMETER FOR NUMERICAL SIMULATIONS

| | MODEL | | | | | | | | | | | | | | | | |
|---|---|---|---|---|---|---|---|---|---|---|---|---|---|---|---|---|---|
| PARAMETER | 1 | 2 | 3 | 4 | 5 | 6 | 7 | 8 | 9 | 10 | 11 | 12 | 13 | 14 | 15 | 16 | 803 |
| $R_a$ | 1.2 | 8 | 1.2 | 8 | 2 | 2 | 2 | 8 | 8 | 8 | 12 | 12 | 12 | 2 | 2 | 2 | 8 |
| $R_{max}$ | 30 | 30 | 30 | 30 | 30 | 30 | 30 | 30 | 30 | 30 | 30 | 30 | 30 | 30 | 18 | 12 | 12 |
| $V_{max}$ | 50 | 50 | 50 | 50 | 50 | 50 | 50 | 50 | 50 | 50 | 50 | 50 | 50 | 50 | 50 | 50 | 50 |
| $X(r)$ | 5e3 | 5e3 | 5e3 | 5e3 | 5e2 | 5e3 | 5e3 | 5e2 | 5e3 | 5e4 | 5e2 | 5e3 | 5e4 | 9e3 | 9e3 | 9e3 | 3e4 |
| $R_{orb}$ | 30 | 30 | 10 | 10 | 10 | 10 | 10 | 10 | 10 | 10 | 10 | 10 | 10 | 10 | 10 | 10 | 10 |
| $R_{O*}$ | 3 | 3 | 3 | 3 | 3 | 3 | 3 | 3 | 3 | 3 | 3 | 3 | 3 | 3 | 3 | 3 | 3 |
| $F_{O*}$ | 50 | 50 | 50 | 50 | 50 | 50 | 50 | 50 | 50 | 50 | 50 | 50 | 50 | 50 | 50 | 50 | 50[a] |

[a] $F_{wr} = 1$ in models 1–16 and $F_{wr} = 30$ in model 803, which is illustrated in Fig. 6.

In Table 2 we list the parameters which were used for the model simulations we will discuss in the following sections.

### 3.1. *Velocity Structure Diagnostics*

The initial question we wish to address concerning the velocity law within the W-R wind is the physical extent over which the wind is undergoing an acceleration. Thus, as mentioned above, the simplest approach is to use a piecewise linear velocity law, where $v(r) \sim r$ up to a distance $R_a$, after which point $v(r) =$ constant. We emphasize that the use of this law is justified at this stage insofar as our objective is to derive diagnostics to differentiate between accelerating and constant velocity flows. Thus, according to this law the wind is undergoing a constant acceleration between $r = r_*$ and $R_a$. One important point to note is that, as one increases the acceleration radius, $R_a$, while holding the terminal speed $V_{max}$ constant the radial velocity gradient decreases, and the Sobolev optical depth along the line of sight to the observer [i.e., $\chi(r)/(dV_z/dz)$] increases. Thus, one expects that a very extended acceleration zone will lead to strong absorption during atmospheric eclipses. On the other hand, a very small $R_a$ will lead to a relatively optically thinner wind in the accelerating zone. Hence, a priori, we might expect qualitative differences in the wavelength-dependent absorption during the atmospheric eclipses. In addition, the presence of wind material traveling at a constant velocity in the region $R_a < r < R_{max}$ will lead to absorption at wavelengths corresponding to terminal speeds. The larger the zone of constant velocity is, the larger is the opacity. Note that in this region the Sobolev approximation breaks down since $dV_z/dz \approx dv(r)/dr = 0$.

In Figure 2 the above qualitative description is confirmed. In this figure we compare the phase-dependent profile differences for two velocity laws, and under two different binary scenarios. The top panels illustrate the results for the case of a binary system in which the O-star's orbital radius is larger than the maximum extent of the line-emitting region (Models 1 and 2), while the bottom panels refer to the case of an O-star which is orbiting within the line-forming region (Models 3 and 4). The panels on the left correspond to model runs with a "fast" velocity law ($R_a = 1.2$), while those on the right correspond to model runs with a "slow" velocity law ($R_a = 8$). Each curve in this figure can be regarded as representing the absorption profile produced in the column of wind projected onto the O-star at impact parameter $p$.

#### 3.1.1. *O-Star Orbit Larger Than the Line-forming Region*

In this case, the column of wind projected upon the O-star is symmetrical with respect to the $p$-axis, and equal amounts of absorption occur on both sides of line center. As the O-star moves along its orbit, from phase $t_0 = 0.75$ to $t_0 = 0.99$, the line of sight from the observer to the O-star traverses columns of wind where the line of sight component of the expansion velocity is growing, both to the "red" as well as to the "blue." This leads to an increase in the width of the absorption with increasing phase. In addition, given that the orbital impact parameter is becoming smaller, there is an increase in the density of the wind throughout the column, producing stronger absorption with increasing phase.

For impact parameters $p/r_* = 24.3$, 19.1, and 14.5, the phase-dependent changes are the same in model 1 (Fig. 2*a*) and model 2 (Fig. 2*b*) because in both cases the line of sight to the O-star is traversing wind which is expanding at a constant velocity. The shape of these profile differences is boxlike, with the strongest absorption occurring at the largest velocities sampled.

When $p = 7.5r_*$, the column of W-R wind of model 2 which is projected onto the O-star contains accelerating material. The curve at this phase no longer is the same as the corresponding curve of model 1. At $p = 3.8r_*$, a very large fraction of the column of wind of model 2 projected onto the O-star is undergoing acceleration. The profile difference is parabolic shaped and has a strong minimum near line center. In model 1 at this impact parameter the constant-velocity wind is still eclipsing the O-star (since $R_a = 1.2r_*$), and the qualitative shape of $\Delta F$ remains the same as for previous impact parameters. In both cases, models 1 and 2, and particularly at $P = 3.8r_*$, prominent "spikes" appear at $+V_\infty$ ("red") and $-V_\infty$ ("blue") positions on the profiles. These "spikes" are formed in the constant-velocity portions of the wind ($r > R_a$) being projected onto the O-star.

From the above, we derive two diagnostics which can be applied for constraining the wind velocity structure:

1. If the column of W-R wind which lies along the line of sight to the O-star during atmospheric eclipse is expanding with a constant (radial) velocity, the profile difference will display a box-shaped figure. If the column of W-R wind which lies along the line of sight to the O-star is undergoing a (radial) acceleration, the profile difference will display a parabolic shape.

2. The presence of absorption spikes at the edges of the profile difference are indicative of wind contained in the column which is expanding with a constant velocity. If both $+V_\infty$ and $-V_\infty$ spikes are present at equal intensities, then the wind has achieved terminal speed within the orbital radius.

#### 3.2.2. *O-Star Orbit within the Line-forming Region*

The lower panels of Figure 2 (models 3 and 4) correspond to the case in which the O-star is orbiting within the W-R line-

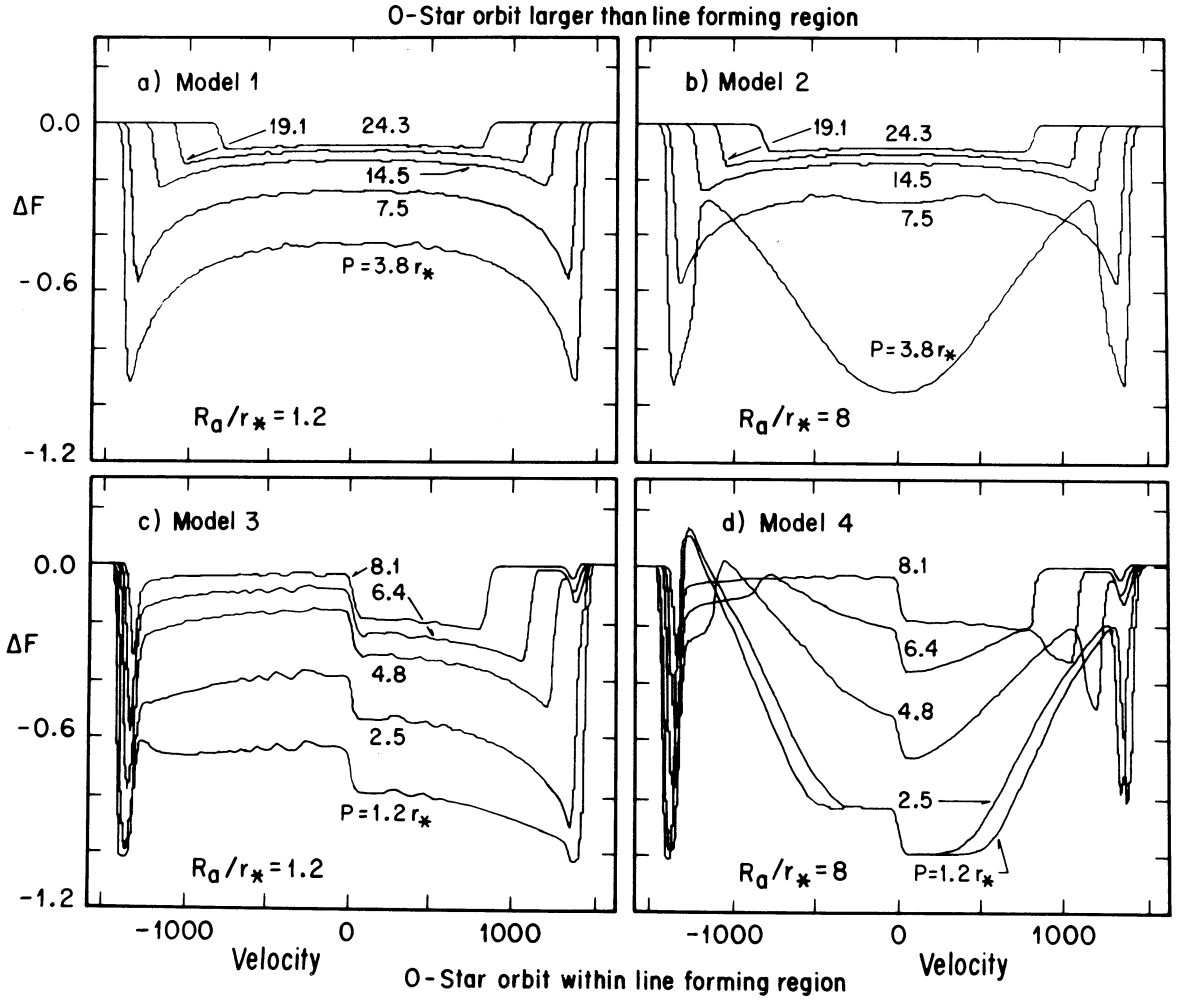


FIG. 2.—Differenced synthetic emergent line profiles predicting the phase-dependent variations in a rapidly accelerating ($R_a = 1.2$; Figs. 2*a* and 2*c*) and a slower ($R_a = 8$; Figs. 2*b* and 2*d*) wind. The abscissa is wavelength displacement in observer-frame velocity units. The different curves correspond to different orbital impact parameters, as marked. When the wind projected on to the O-star is accelerating, the profile differences have a parabolic shape (Figs. 2*b* and 2*d*) as opposed to the case of a constant wind where the profile differences are more box-shaped (Figs. 2*a* and 2*c*).

forming region. The structure of the wind, and all other parameters are the same as in models 1 and 2.

Both models 3 and 4 produce *asymmetrical* profile differences. This is due to the fact that at the reference phase ($t_0$), the O-star already lies behind a portion of the W-R line-forming region, and this region is already producing an absorption. At $t_0$ the entire column of material projected onto the O-star is approaching the observer, so this absorption occurs only at negative velocities in the line profile (not profile difference!). At other phases, part of the column of material projected onto the O-star now contains velocity components approaching the O-star (and receding from the observer), leading to absorption on the positive side of the profile, with little increase in the absorption at the negative side of the profile. Thus, when subtracting the profile at phase $t_0$ from the profile at phase $t$, the largest difference occurs on the "red" side. Thus, we arrive at a third diagnostic:

3. If the O-star's orbit lies within the line-forming region, the profile differences will be asymmetric, with an abrupt jump near line center.

Note that the blue "spike" is not subtracted out. This is due to the fact that, at the reference phase, the constant-velocity region is expanding at an angle with respect to the line of sight, and the cylinder in which the absorption takes place includes material moving at various directions outward from the O-star, so that the absorption is broad. Furthermore, all of these velocity components are smaller than the terminal speed. But as the O-star goes around behind the W-R, the spread in velocity components becomes smaller, and the absorption becomes more and more nearly monochromatic, while it moves toward the maximum expansion velocity (i.e., toward shorter wavelengths). Thus, when the two profiles are subtracted, the velocity displacement between the "spikes" at both orbital phases produces a residual absorption.

The general features of the profile differences for a "fast" and a "slow" velocity law, as observed for models 1 and 2, respectively, are reproduced, even though the shapes are asymmetrical, and diagnostics (1) and (2) still hold.

Note also that the "red" spike in Figure 2*d* does not become as strong as the corresponding "blue" spike simply because there is not as much material traveling at constant velocity toward the O-star as there is moving away from it. If $R_a > R_{orb}$, the "red" spike would never be observed. (This is, of course, under the assumption that the O-star does not alter the W-R wind structure.)

In the following sections we'll limit the discussion to the case of the O-star orbiting within the line-forming region.

### 3.2. *Dependence on the Opacity Factor X(r)*

In this section we will explore the degree to which the diagnostics for the velocity structure of the W-R wind derived in the previous section, depend upon the opacity factor $X(r)$. The opacity factor as used in the code is a nondimensional parameter defined such that

$$\tau = \int \frac{X(r)}{[v(r)/v_{\rm th}](r/r_*)^2}\,\phi[x - v_z(z)]d\left(\frac{z}{r_*}\right). \quad (8)$$

Thus, $X(r)$ can be related to the mass-loss rate $\dot{M}$, and the radius at which the acceleration starts $r_*$ by

$$X(r) = \frac{\dot{M}}{r_*}\frac{\sigma}{4\pi\mu m_{\rm H} v_{\rm th}} f_{ijk}(r). \quad (9)$$

Here, $\mu$ is the mean molecular weight, $m_{\rm H}$ is the mass of hydrogen, $v_{\rm th}$ is the thermal speed, $\sigma$ is the cross section for the transition, and $f_{ijk} = N_i/N_{\rm tot}$ represents the number density of ions in the appropriate energy level which can give rise to the line transition under consideration with respect to the total number density. Adopting as typical values $\mu = 2$, $v_{\rm th} = 20$ km s$^{-1}$, $\sigma = 5 \times 10^{-17}$ cm$^2$, $\dot{M} = 10^{-5}\,M_\odot$ yr$^{-1}$, we get

$$X(r) = 5.8 \times 10^9 \frac{(\dot{M}/10^{-5}\,M_\odot\ {\rm yr}^{-1})}{r_*/R_\odot} f_{ijk}. \quad (10)$$

Models 5–13 illustrated in Figure 3 probe the behavior of the profile differences, as a function of increasing opacity $X(r)$. The three values of $X(r)$ used can be associated with optically thin ($X = 500$), intermediate opacity ($X = 5000$), and optically thick ($X = 50{,}000$) lines, and correspond approximately to values of $f_{ijk}$ in the range $10^{-7}$ to $10^{-5}$. The computations were performed with three different velocity laws: $R_a/r_* = 2$, 8, and 12. The extent of the line-forming region is $R_{\rm max} = 30r_*$, and the orbital separation was fixed to $R_{\rm orb} = 10r_*$, so the O-star lies within the line-forming region.

We find that one can always discriminate between constant and accelerated flows, according to diagnostic (1) as long as the line is not optically thick. When the line is optically thick, the

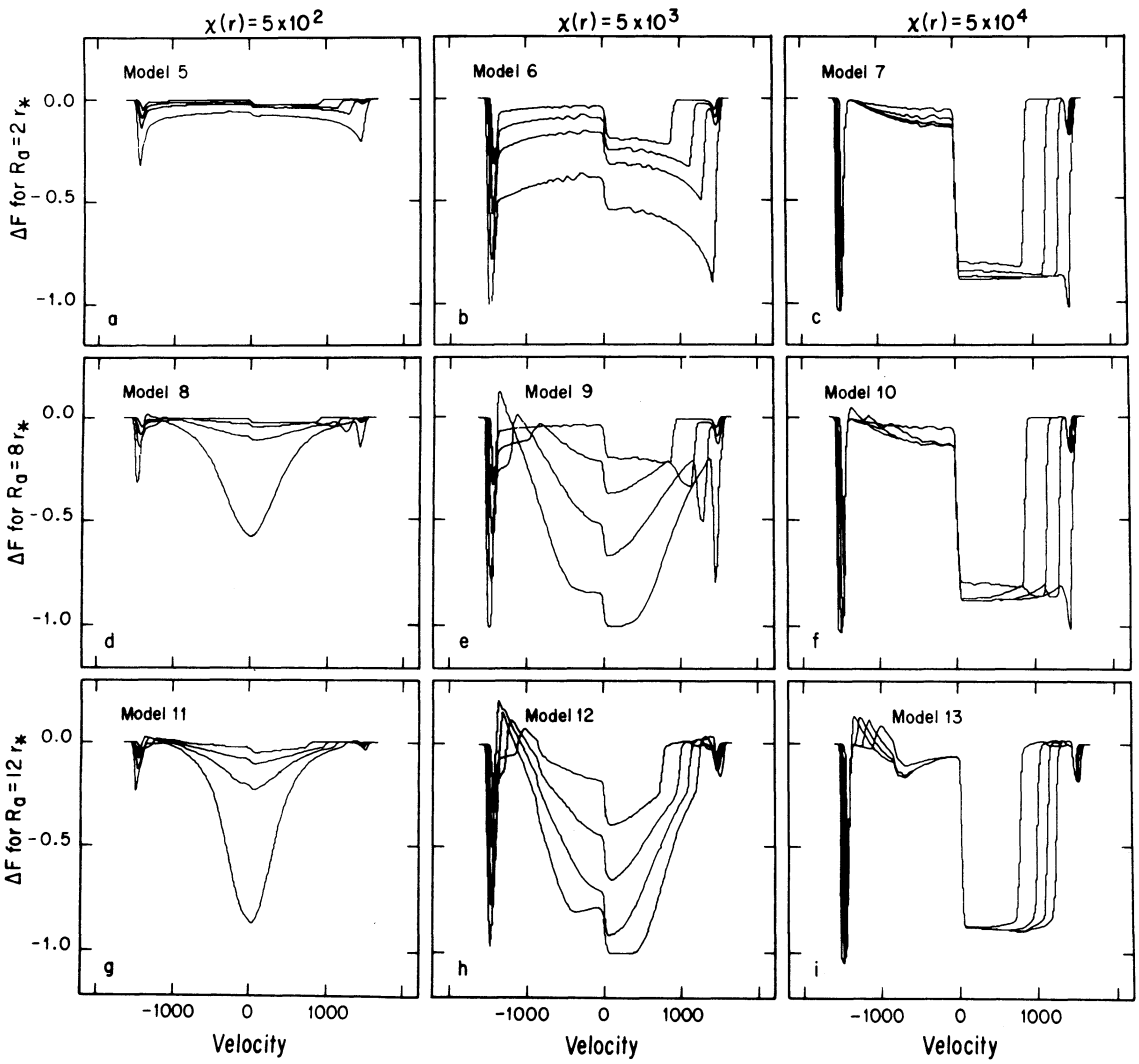


FIG. 3.—Comparison of the models for different opacity factors, $X(r)$, and acceleration radii, $R_a$, for the case of the companion orbiting within the W-R wind. Larger $R_a$'s imply more extended accelerating regions and smaller velocity gradients. Note that at $X(r) = 5 \times 10^4$ the profile differences become degenerate due to the large optical depth of the line (Figs. 7, 10, and 13).

differences are insensitive to orbital phase changes, beyond some orbital phase. The first portions of the line profile to saturate are, evidently, those formed in wind regions of largest density; i.e., in the region close to the star. This can be seen in Figures 3*c*, 3*f*, and 3*i*, where the curves corresponding to different orbital phases tend toward "degeneration" at all wavelengths except at the "red" edges.

When a line is optically thick at all wavelengths, diagnostic (1) is no longer applicable, and little information regarding the presence of an accelerating region can be extracted. However, diagnostics (2) and (3) still pertain.

For optically thin and intermediate opacity cases, although there is no qualitative dependence of the profile differences with opacity, there is a quantitative one. For example, in the case of a "fast" velocity law, where most of the line is forming in a wind expanding with a constant velocity, the profile differences for models with $X = 500$ can be scaled to those with $X = 5000$ by simply multiplying the intensity at all wavelengths by a factor of 5. In the case of a "slow" wind, where most of the line-forming region is contained in the accelerated flow, the scaling is wavelength-dependent, and the difference profiles become broader with an increasing opacity.

Hence, for non–optically thick cases, the variation of the line depth with impact parameter gives a direct constraint on the number density of absorbers in a very localized region of the wind.

### 3.3. *Dependence on the Extent of the Line-forming Region, $R_{max}$*

The extent of the line-forming region affects the width of the "spikes" which appear at $\pm V_\infty$. In Figure 4 we illustrate how the width of these features increases as $R_{max}$ decreases. This increase in width is a result of the manner in which the $V_z$ projected onto the O-star, in the regions where $v(r)$ = constant, increases. In the limit when $R_{max} < R_{orb}$, the shapes of the profiles of Figures 2*a* and 2*b* will be recovered.

### 3.4. *Dependence on the Radius of the O-Star*

There is no qualitative change in the difference profiles for different O-star radii. There is a quantitative difference, which goes approximately as $R_{O*}^2$, and which can be understood in terms of a greater quantity of wind material being projected onto the more extended O-star continuum source, and thus leading to a stronger absorption.

## 4. COMPARISON WITH THE OBSERVATIONS

The wind eclipse model predicts that the P Cygni–type profiles in binary systems should undergo phase-dependent variations, consisting in enhanced absorption. The difference between observed profiles at phase $t$ and a reference phase $t_0$ should be similar to one of the model differences illustrated in Figures 2–4 if the model is applicable.

### 4.1. *The Data*

We have chosen to use the N IV 1718 Å line in the *IUE* high-dispersion spectra of the WN5+06 binary system V444 Cyg to illustrate how the simple eclipse model presented in this paper can be applied. This line was chosen because it is known to display variations with the orbital phase in at least seven WN binary systems in which this effect has been sought (Koenigsberger & Auer 1985; Moffat et al. 1989). V444 Cyg was selected because it is the best studied WN binary system, with repeatedly determined orbital parameters. Although we will adopt the "canonical" parameters usually used for V444 Cyg (specifically $R_{wr} = 3\ R_\odot$, $R_{O*} = 10\ R_\odot$), it is important to note that a recent analysis by Hamann & Schwartz (1992) has yielded quite different results ($R_{wr} \approx 6\ R_\odot$ and $R_O \leq 5\ R_\odot$; but see also Cherepashchuk et al. 1994).

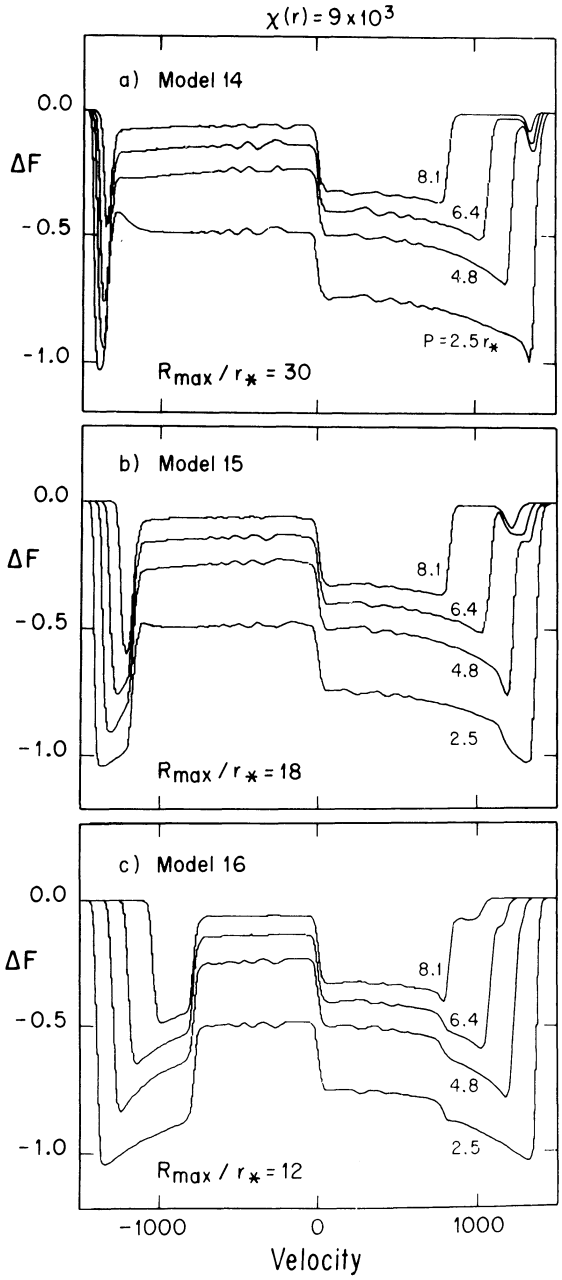


FIG. 4.—Example of the effect that $R_{max}$ has on the width of the "blue spike." As $R_{max}$ is changed from $30r_*$ to $12r_*$, the width of this feature increases.

Although the archives of *IUE* data contain a large number of spectra of V444 Cyg, many of the images were unfortunately poorly exposed in the continuum, to avoid saturation of the He II 1640 Å line. Thus, we have selected those with the longest exposure times since the best possible signal-to-noise ratio is required at continuum levels and below. In Table 3 we list those images used in our present analysis. These spectra were not all obtained during the same orbital cycle, and are basically the same data used by Stevens (1993).

TABLE 3

*IUE* OBSERVATIONS OF V444 CYGNI

| SWP | Observer[a] | Phase | $p(R_\odot)$ | $p(r_*)$ | RV(km s$^{-1}$) |
|---|---|---|---|---|---|
| 26000..... | SB88 | 0.74 | 30 | 10.3 | −289. |
| 26065..... | SB88 | 0.88 | 25 | 8.6 | −194. |
| 26066..... | SB88 | 0.92 | 19 | 6.5 | −132. |
| 26030..... | SB88 | 0.95 | 13 | 4.5 | −79. |
| 26031..... | SB88 | 0.99 | 8 | 2.7 | +4 |
| 26007..... | SB88 | 0.00 | 7 | 2.4 | +15 |
| 26008..... | SB88 | 0.04 | 12 | 2.7 | +91 |
| 24745..... | UF87 | 0.08 | 19 | 6.5 | +162 |
| 25990..... | SB88 | 0.08 | 19 | 6.5 | +162 |
| 25994..... | SB88 | 0.53 | ... | ... | −42 |

[a] SB88: Shore & Brown 1988; UF87: Underhill & Fahey 1987.

After extraction of these data from the *IUE* archives, they were processed with the standard IUESPEC routine at the GSFC/RDAF. They were then smoothed with a five-point running average. These data were then further processed by applying a Wiener filter, with a window size of 11 points, to thus additionally smooth the data. Despite this effort, the data are very noisy. The spectra were normalized to the nearby level of the continuum of SWP 26000 (i.e., $F_c = 1.6 \times 10^{-12}$ ergs cm$^{-2}$ s$^{-1}$ Å$^{-1}$).

In order to transform the wavelength scale to the velocity in the reference frame of the W-R star, we have used the radial velocities listed by Münch (1950). That is, we adopt a semi-amplitude for the velocity curve of 305 km s$^{-1}$. In addition, for the velocity of the rest frame of the system (i.e., gamma velocity) we have adopted the average value which results from the N IV 4058 Å and the N V 4603–21 Å radial velocity curves, that is, $\frac{1}{2}[\gamma(\text{N IV}) + \gamma(\text{N V})] = \frac{1}{2}(-40 + 70) = +15$ km s$^{-1}$. Note that this value of the $\gamma$ velocity is in good agreement with the value obtained from the O-star photospheric absorption lines [$\gamma$(O-star) = +10 km s$^{-1}$]. We attribute the different values of the $\gamma$ velocity derived for different W-R emission lines to asymmetries which are intrinsic to the particular lines. Thus, the transformation to the W-R rest frame applied to each spectrum is the negative of the radial velocity (RV) at that phase: RV($t$) = 305 × sin ($2\pi\phi$) + 15 km s$^{-1}$. The values of RV used are listed in the sixth column of Table 3.

The orbital impact parameter changes as a function of orbital phase $\phi$, and is defined as

$$p = a[\sin^2(2\pi\phi) + \cos^2(2\pi\phi)\cos^2 i]^{1/2},$$

where $a$ is the orbital separation, and $i$ is the inclination. We adopted the values of $a \sin i = 35.4\ R_\odot$ and $i = 78°$ from Münch (1950). These values differ slightly from more recent determinations (Underhill, Yang, & Hill 1988; Acker, Prévot, & Prévot 1989). In the fourth column of Table 3 we list the orbital impact parameters corresponding to the *IUE* observations used here.

Once each profile was shifted to the rest frame of the W-R, the difference between profiles was computed using SWP 26000 as the spectrum at the reference phase; i.e., $\phi_0 = 0.74$. Note that this phase is nearly at the elongation at which the O-star is receding from the observer and corresponds to $t_0$ as defined for the model simulations. In Figure 5 we present the profiles at $\phi_0 = 0.74$ and at $\phi = 0.95$. The enhanced absorption at phase 0.95 with respect to elongation is evident.

The *IUE* spectra we have correspond to orbital phases just prior to and just after primary minimum, and hence permit a comparison of the atmospheric eclipses on symmetrical sides of the W-R wind with respect to phase 0.00. For example, there are spectra at phases 0.92 and 0.08, both of which correspond to the same impact parameter $p = 19\ R_\odot$. It is interesting to note that, within the noise levels of the current data, profile differences for the same impact parameter are not distinguishable. Hence, we have averaged together the profile differences corresponding to similar impact parameters. With this, the differences for impact parameters $p = 24, 19, 12, 7\ R_\odot$ were constructed: difp24 (SWP 26065); difp19 (SWP 26066+24745+25990); difp12 (SWP 26030+26008); and difp7 (SWP 26031+26007). These are shown in Figure 6, on a velocity scale.

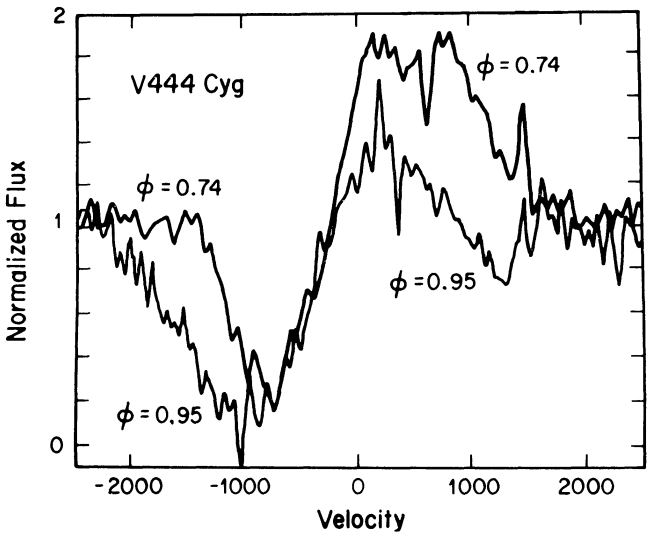


FIG. 5.—Observed profiles of the N IV 1718 Å line in V444 Cyg at orbital phases 0.74 and 0.95. The decreased intensity at phase 0.95, phase at which the O-star is on the "far" side of the W-R wind, is mostly a result of the wind eclipse.

The general features of the differences plotted in Figure 6 are as follows:

1. There are two troughs: one ranging in velocity from 0 to +1200 km s$^{-1}$, and the other (the "blue spike") which is centered at −1500 km s$^{-1}$ and becomes stronger as $p$ decreases.
2. The maximum radial velocity displayed by the wind of the "blue spike" lies between −1800 and −1900 km s$^{-1}$.
3. There is a "red" minimum, centered first at +700 km s$^{-1}$ at $p = 19\ R_\odot$ and moves out to about +900 km s$^{-1}$ at $p = 7\ R_\odot$.
4. There is a slight increase in the depth of the troughs between $p = 24\ R_\odot$ and $p = 19\ R_\odot$. However, there is no measurable change in the depth of the troughs between $p = 19\ R_\odot$ and $p = 7\ R_\odot$.
5. There is no change, as a function of orbital phase, in the intensity level in the region between the two troughs; i.e., in the velocity range −1100 to −200 km s$^{-1}$.

### 4.2. *Constraints on the Wind Structure*

From a purely qualitative comparison with the models, the above data provide the following information:

1. The O-star orbit lies within the N IV 1718 Å line-forming region, given the asymmetry in the profile differences. Hence, $R_{\max}$(N IV 1718 Å) ≥ 36 $R_\odot$.

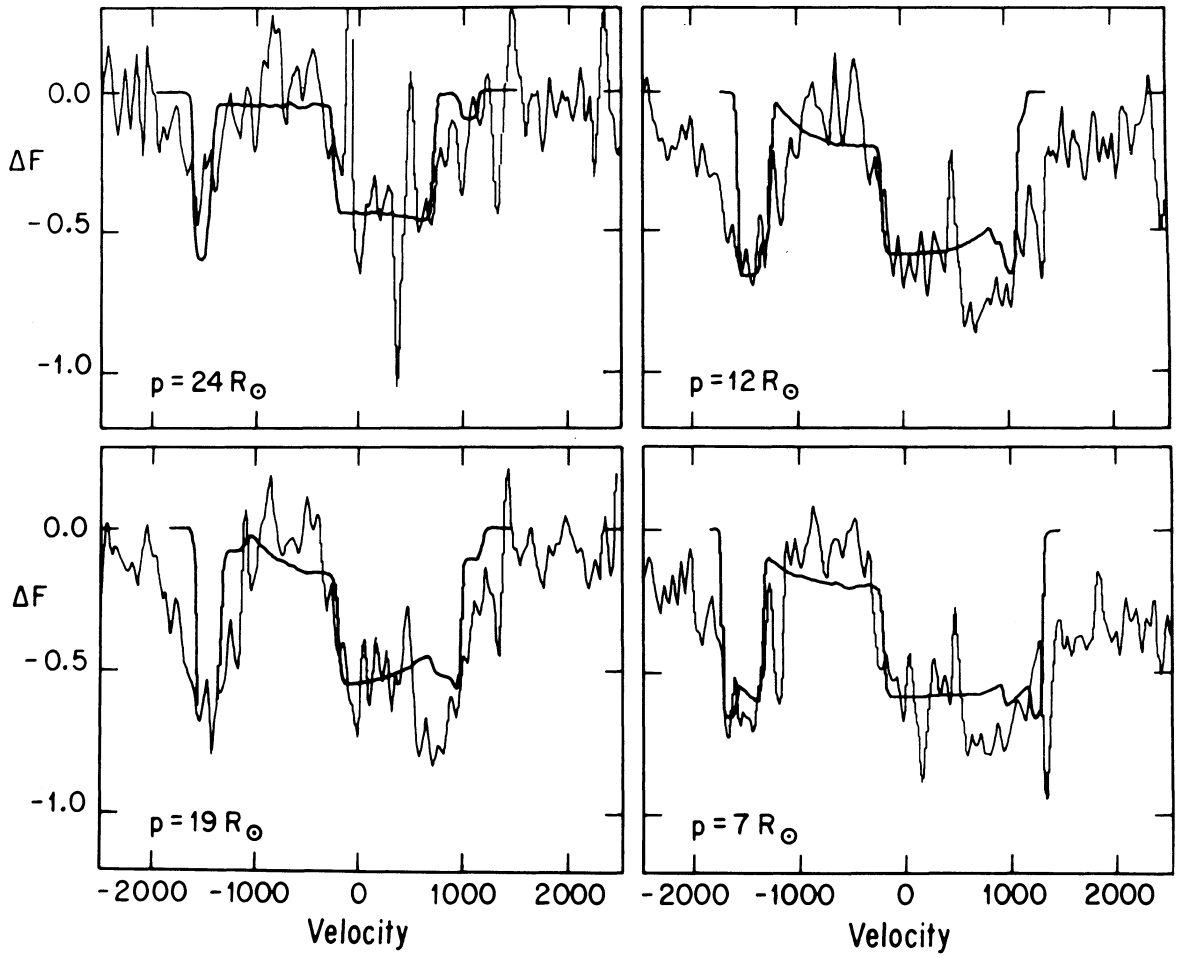


FIG. 6.—Differences of the spectra at orbital impact parameter $p/R_\odot$ = 24, 19, 12, and 7 with respect to the spectrum at phase 0.74($p$ = 32 $R_\odot$) in V444 Cyg. Superposed on each observed difference is the predicted difference from model 803, at the corresponding orbital impact parameter. The velocity scale of the model output has been converted to absolute velocity with $v_{th}$ = 30 km s$^{-1}$. To achieve a good fit, the model curves were shifted by −200 km s$^{-1}$, which accounts for probable asymmetries in the wind due to the presence of the O-star, which are not contemplated in the code. The excess red absorption in the data, with respect to the synthetic profile difference for $p$ = 19, 12, and 7 $R_\odot$ may be due to the wind-wind collision, where the W-R wind structure is altered. The effect of the wind-wind collision is small, relative to that of the wind eclipse.

2. The terminal speed of the W-R wind lies within the range −1500 to −1900 km s$^{-1}$.

3. The "blue spike" indicates the presence of a flow at constant velocity, within the N IV 1718 Å line-forming region. This means that, within our simplistic flow model, we can state that the wind stops accelerating at distances from the W-R core where excited states of N IV still prevail. The one caveat to this assertion concerns the question of whether radiation-driven instabilities (Castor 1987; Owocki 1991 and references therein) permeate the wind and what their impact is on the line profiles. We shall return to this question below.

4. Because there is no significant change in $\Delta F$ for $p \leq 19\ R_\odot$, we conclude that almost the entire line (i.e., throughout its wavelength range) is optically thick for $p \leq 19\ R_\odot$. Hence, we cannot derive information regarding the velocity structure within this radius by using this particular line.

In Figure 6 we have superposed one of the optically thick models which reproduces the general features of the data, and which provides us with further, more quantitative information:

5. The width of the "blue spike" requires that the extent of the line forming region, $R_{max}$, be smaller than $12r_*$, assuming an orbital radius of $R_{orb} = 10r_*$. If $R_{max}$ is much larger than 12, the "blue spike" is too narrow. In the case of a model with $R_{orb} = 5r_*$, then $R_{max} < 7r_*$. Both of these options (which depend upon the value of $r_*$ adopted) imply $R_{max}$(N IV 1718 Å) $\approx 40\ R_\odot$. This result is independent of the velocity law used in the model, as long as $R_a < R_{orb}$. However if wind-driven instabilities permeate the wind, these could provide a mechanism for turbulent broadening of this "blue spike."

6. The ratio of continuum intensities required to fit the depth of the troughs is $F_{wr}/F_O$ = 0.5–0.6.

The depression at +800 km s$^{-1}$, which is stronger than the model prediction, may be indicating the presence of (slower-than-terminal) constant velocity wind in the region which lies between the two stars and may be the result of the wind-wind collision. It is important to note that the presence of a wind-wind collision region does *not* affect in anyway conclusions which are based on the "blue spike" since this feature is formed in the W-R wind far from the O-star's effects.

### 4.3. *Constraints on the Radius of the W-R Core*

The most critical parameter to the modeling effort is the value of $r_*$, which until recently was systematically assumed to

be 2.9 $R_\odot$, following the analysis by Cherepashchuk, Eaton, & Khaliullin (1984). However, a reanalysis of the light curve combined with modeling of the helium spectrum by Hamann & Schwartz (1992) has yielded $r_* \approx 6\ R_\odot$ and $R_{O*} \approx 3$–$5\ R_\odot$. This means that in terms of the stellar radius, the impact parameters for the data shown in Figure 5 correspond either to (8, 6.3, 4., and $2.3r_*$) or (4, 3.2, 2., and $1.2r_*$), for $r_* = 3\ R_\odot$ and $6\ R_\odot$, respectively. Equation (10) allows us to derive the value of $r_*$, given independently determined values of $\dot{M}$ and $f_{ijk}$, and values of $X(r)$ obtained from modeling the line profile differences. A very rough estimate of $f_{ijk}$, given $N(\text{nitrogen})/N_{\text{total}} \approx 3 \times 10^{-3}$ (Hillier 1988), and assuming that one-third of $N$ is N IV and that the abundance of N IV ions populating the lower level of the 1718 Å transition is $10^{-2}$, yields $f_{ijk} \approx 10^{-5}$. If $\dot{M}_{\text{V444}} = 2 \times 10^{-5}\ M_\odot\ \text{yr}^{-1}$ and given $X(r) = 3 \times 10^4$ from the model, we obtain $r_* \approx 3.8\ R_\odot$. This value would correspond, within the framework of our analysis, to the radius at which acceleration commences. We must emphasize that this is a very rough estimate, which we present merely to illustrate the potential of the present techniques.

## 5. CONCLUSIONS

We have applied a new very efficient approach to the radiative transfer problem, valid even for nonmonotonic velocity fields, to produce computer simulations of the line profile variations induced by wind eclipses in binary systems. In this first exploratory stage, we have restricted the analysis to a simple flow model which consists of an initially accelerating wind, up to a radius $R_a$, followed by a constant velocity flow, up to a maximum radius for the line forming region, $R_{\max}$. The additional simplifying assumptions are (1) the line is formed by pure absorption; (2) no alterations of the dynamics of the W-R wind by the O-star companion; (3) no emission line arising in the O-star; and (4) constant ionization structure throughout the particular line-emitting region.

We find that the models predict different phase-dependent variations for different wind structures, the velocity law being the most critical parameter determining these variations, as long as the line is not optically thick. The models provide three diagnostics which can be applied qualitatively to the data and allow one to determine whether (1) the column of W-R wind projected onto the O-star companion at each orbital phase during wind eclipse is undergoing an acceleration or is traveling at a constant speed; (2) whether the line being studied is formed in both the accelerating and the constant velocity regions of the wind, or only in one of these regions; and (3) whether the extent of the line-forming region is larger than, or smaller than the orbital radius. By modeling the profile variations, additional information which can be obtained includes the values of $R_{\max}$ and of the opacity factor, $X(r)$.

Under the very simplified conditions explored in this paper, the first diagnostic will immediately impose constraints on the extent (in absolute units) of the accelerating region of the W-R wind, without any need for profile fitting. However, on the more general case in which scattering, the contribution of the line emission arising in the vicinity of the companion O-star, or a nonconstant ionization structure must be analyzed, this diagnostic may not be as straightforward to apply and modeling of the profile variations will be necessary.

The numerical value of the opacity factor, $X(r)$, which is arrived at by modeling the profile variations, provides an independent measure of the parameter ratio $\dot{M}/r_*$, if the number density of the absorbers is known. Given that the mass-loss rate can be determined from other methods, $X(r)$ provides a semiempirical constraint on the value of $r_*$. This radius, according to the model, corresponds to the position at which the acceleration of the wind commences. Since the continuum is believed to the optically thick at the base of the flow, and the extent of this optically thick continuum region is not known, it has not been possible to constrain $r_*$ via other modeling or observational efforts. If the acceleration starts on the surface of the W-R core, then $r_*$ can be associated with the radius of the W-R star, $R_{\text{wr}}$. Even in the case of V444 Cyg, the best studied W-R star, the various determinations of $R_{\text{wr}}$ lie in the range 2.6–6 $R_\odot$ (cf. Hamann & Schwartz 1992). Thus, the use of $X(r)$ as described above for deducing $r_*$ seems very attractive.

For illustrative purposes, we applied the method to the line of N IV 1718 Å in V444 Cyg. The line is shown to be optically thick out to distances between 19 and 24 $R_\odot$, and thus no information can be derived regarding the extent of the acceleration zone in the W-R wind. However, applying diagnostics (2) and (3) we are able to conclude that the extent of the N IV 1718 Å line-forming region is slightly larger than the orbital radius and that there is wind traveling with a constant (radial) velocity within this line-forming region. According to our idealized flow model, the evidence for a constant velocity flow in the N IV 1718 Å region would indicate that the wind has achieved its terminal velocity within this region. However, if there are radiation-driven instabilities which propagate outward as shocks within the accelerating region of the wind, the nonmonotonic velocity structure could give rise to the feature we have defined as the "blue spike." This question will be addressed at the next stage of our analyses of the models. From an observational standpoint, it is crucial to perform an analysis of the variations in other N IV lines, such as N IV 3483, 4058, and 6380 Å, which should be optically thinner and provide better constraints on the acceleration region in the wind of V444 Cyg. In addition, higher quality data of N IV 1718 Å should be obtained for V444 Cyg and other binary systems.

The final point we wish to make is that we find it very significant that N IV 1718 Å is optically thick out to about 20 $R_\odot$. When the optical depths of lines are very large, the diffuse force will make an important contribution to the acceleration of the winds (Pauldrach 1987). Puls (1987), Puls & Pauldrach (1990), and Springmann (1994) find it probable that the final acceleration of W-R star winds takes place far out in the wind, under the assumption of strong absorption in the lines. If N IV 1718 Å can be regarded as representative of those lines driving the wind, this means that the acceleration zone should extend to 20 $R_\odot$ in V444 Cyg. If $r_* = 2.9\ R_\odot$, this would mean that $R_a = 6.9r_*$.

G. K. thanks L. Jacobs for providing UNIX computing tools and A. F. J. Moffat for a critical reading of the manuscript. We thank an anonymous referee for helpful comments and suggestions, and the *IUE* GSFC/DAC staff for their continuing support across networks and countries. This work was concluded while G. K. was a visiting scientist at STScI; the investigation was supported in part by the US Department of Energy, by NASA grant WRKLA, and by grants IN104591 from the DGAPA/UNAM, and 1160E from CONACYT.

REFERENCES


Abbott, D. C., Bieging, J. H., Churchwell, E., & Torres, A. V. 1986, ApJ, 303, 329
Acker, A., Prévot, M.-L., & Prévot, M. 1989, A&A, 226, 137
Annuk, K. 1991, in IAU Symp. 143, Wolf-Rayet Stars and Interrelations with Other Massive Stars in Galaxies, ed. K. A. van der Hucht & B. Hidayat (Dordrecht: Kluwer), 245
Auer, L. H., & Dickel, J. R. 1994, ApJ, in press
Barlow, M. J., Smith, L. J., & Willis, A. J. 1981, MNRAS, 196, 101
Castor, J. I. 1987, in Instabilities in Luminous Early-Type Stars, ed. H. J. G. L. M. Lamers & C. W. H. de Loore (Dordrecht: Reidel), 159
Cherepashchuk, A. M., Eaton, J., & Khalliulin, Kh. 1984, ApJ, 281, 774
Cherepashchuk, A. M., Koenigsberger, G., Marchenko, S., & Moffat, A. F. J. 1994, A&A, in press
Hamann, W.-R. 1985, A&A, 145, 443
Hamann, W.-R., & Schmutz, W. 1987, A&A, 174, 173
Hamann, W.-R., Schmutz, W., & Wessolowski, U. 1988, A&A, 194, 190
Hamann, W.-R., & Schwartz, E. 1992, A&A, 261, 523
Hillier, D. J. 1983, Ph.D. thesis, Australian National Univ., Canberra
———. 1987a, ApJS, 63, 947
———. 1987b, ApJS, 63, 965
———. 1988, ApJ, 327, 822
———. 1989, ApJ, 347, 392
———. 1991, in IAU Symp. 143, Wolf-Rayet Stars and Interrelations with Other Massive Stars in Galaxies, ed. K. A. van der Hucht & B. Hidayat (Dordrecht: Kluwer), 59
Koenigsberger, G. 1990, A&A, 235, 282
Koenigsberger, G., & Auer, L. H. 1985, ApJ, 297, 255
———. 1991, in IAU Symp. 143, Wolf-Rayet Stars and Interrelations with Other Massive Stars in Galaxies, ed. K. A. van der Hucht & B. Hidayat (Dordrecht: Kluwer), 179
Kopal, Z., & Shapley, M. 1946, ApJ, 104, 160
Kudritzki, R. P., & Hummer, D. 1990, ARA&A, 28, 303
Lou, D., McCray, R., & Mac Low, M. 1990, ApJ, 362, 267
Lucy, L. B., & Abbott, D. C. 1993, ApJ, 405, 738
Mihalas, D. 1978, Stellar Atmospheres (2d ed.; San Francisco: Freeman)
Moffat, A. F. J., Koenigsberger, G., & Auer, L. H. 1989, ApJ, 344, 734
Münch, G. 1950, ApJ, 112, 266
Owocki, S. P. 1991, in IAU Symp. 143, Wolf-Rayet Stars and Interrelations with Other Massive Stars in Galaxies, ed. K. A. van der Hucht & B. Hidayat (Dordrecht: Kluwer), 155
Pauldrach, A. W. A. 1987, A&A, 183, 295
Pilutskii, O. F., & Usov, V. V. 1976, Soviet Astron., 20, 2
Puls, J. 1987, A&A, 184, 227
Puls, J., & Pauldrach, A. W. A. 1990, in Properties of Hot Luminous Stars, ed. C. D. Garmany (ASP Conf. Ser., 7), 203
Reimers, D. 1987, in IAU Symp. 122, Circumstellar Matter, ed. I. Appenzeller & C. Jordan (Dordrecht: Kluwer), 307
Schmutz, W., Hamann, W.-R., & Wessolowski, U. 1989, A&A, 210, 236
Shore, S., & Brown, D. N. 1988, ApJ, 334, 1021
Springmann, U. W. E. 1994, A&A, in press
Stevens, I. R. 1993, ApJ, 404, 281
Walborn, N., Nichols-Bohlin, J., & Panek, R. 1985, An *IUE* Atlas of O-Type Spectra (NASA Ref. Publication 1155) (Washington: NASA)
Willis, A. J., et al. 1979, in The First Year of *IUE*, ed. A. J. Willis (London: University College), 394